Iridescent structural coloration in a crested Cretaceous enantiornithine bird from Jehol Biota

Short title: Iridescent structural coloration in a crested enantiornithine bird

Elife digestion: Three-dimensional reconstruction of melanosome organization in an enantiornithine feather crest reveals convergent iridescent coloration.

Authors

Zhiheng Li[1†*], Jinsheng Hu[2†], Thomas A. Stidham[1,3], Mao Ye[2], Min Wang[1], Yanhong Pan[4], Tao Zhao[5], Jingshu Li[1], Zhonghe Zhou[1,6], Julia A. Clarke[7]

1 Key Laboratory of Vertebrate Evolution and Human Origins, Institute of Vertebrate Paleontology and Paleoanthropology, Chinese Academy of Sciences, Beijing 100044, China

2 School of Instrumentation and Optoelectronic Engineering, Beihang University, Beijing 100191, China

3 Department of Biology, Austin College, Sherman, Texas 75090, USA

4 State Key Laboratory for Mineral Deposits Research, School of Earth Sciences and Engineering, Centre for Research and Education on Biological Evolution and Environment and Frontiers Science Center for Critical Earth Material Cycling, Nanjing University, Nanjing 210023, China

5 Institute of Palaeontology, Yunnan Key Laboratory of Earth System Science, Yunnan

University, Kunming 650500, China

6 College of Earth and Planetary Sciences, University of Chinese Academy of Sciences, Beijing 100049, China

7 Department of Earth and Planetary Sciences, Jackson School of Geosciences, The University of Texas at Austin, Texas 78712, USA

†These authors contributed equally

*Correspondence: lizhiheng@ivpp.ac.cn (Z.L.)

Abstract

A combination of sectioning and microscopy techniques, along with the application of finite-difference-time-domain modeling on a fossil feather, results in the novel estimation of the range of iridescent colors from the fossilized melanosome type and organization preserved in the elongate head crest feathers of a new Cretaceous enantiornithine bird. The densely packed rod-like melanosomes are estimated to have yielded from red to deep blue iridescent coloration of the head feathers. The shape and density of these melanosomes also may have further increased the feather's structural strength. This occurrence on a likely male individual is highly suggestive of both a signaling function of the iridescent crest, and a potential behavioral role in adjusting the angle of light incidence to control the display of this iridescent structural coloration.

Introduction

The recognition and study of melanosomes in fossil feathers of non-avialan dinosaurs and birds has added greater complexity to the pattern of their diversity and macroevolution, demonstrating the intertwined evolution of coloration with feather functions across display, thermoregulation, and other uses (Li, Gao et al. 2012, Li, Clarke et al. 2014, Terrill and Shultz 2023). This linkage among colors, structures, and functions early in feather evolution extends even to convergence in iridescent feathers among non-avialan theropods, and it is highly suggestive of commonalities shared among stem and crown birds in terms of their use of colored pigments for camouflage, structural strength, and display (Hu, Clarke et al. 2018, Foth and Rauhut 2020). In a comparative setting with the melanosome feather coloration of living birds, workers have endeavored to reconstruct the colors of fossil feathers using quantitative means focused predominantly on melanosome geometry and density, and the results point to the fossilized melanosomes having produced patterns of black, brown, rufous, grey, and other colors (Vinther, Briggs et al. 2008, Li, Gao et al. 2010, Zhang, Kearns et al. 2010, Li, Gao et al. 2012, Peteya, Clarke et al. 2017, Benton, Dhouailly et al. 2019). Furthermore, the specific shape and arrangement of some fossilized feather melanosomes derived from both non-avialan theropod dinosaurs and birds are similar to those required for producing structurally-based iridescent feather coloration in living birds, a case of independent evolution (Stoddard and Prum 2011, Hu, Clarke et al. 2018, Pan, Li et al. 2022).

Feathers serve multiple functions in birds from comprising an insulatory epidermal layer to

forming aerodynamic flight surfaces, and as structures for the containment and display of various pigments. Living birds exhibit diverse feather morphologies and colors, and the significant diversity of known fossil feathers, along with their preserved pigments, points to their past use for camouflage, as well as display and signaling (Prum 2006, Foth and Rauhut 2020, Terrill and Shultz 2023). While the display of most colored feathers are passive and available to any viewer, birds can behaviorally control their signaling through: the erection of feathered ornaments such as the head crest in hoopoes (*Upupa*) or Peacocks (*Pavo*) tails; the exposure of normally hidden brightly colored crown feathers as in Kinglets (*Regulus*); and even the refined control of the black and iridescent coloration in birds such as hummingbirds (Trochilidae) and birds of paradise (Paradisaeidae) (Zi, Yu et al. 2003, Wilts, Michielsen et al. 2014, Stoddard, Eyster et al. 2020). This great variation in structural or iridescent colors results from differences in pigments, their organization, and other structural modifications. For example, the variety of mixed structural colors present in a peacock feather are achieved through changes in the spacing in the keratinous matrix and melanosome organization (Zi, Yu et al. 2003). In addition to the normal range of spectral coloration, hummingbirds can see non-spectral colors as well, and their utility is supported by vision perception experiments (Stoddard, Eyster et al. 2020). The interplay of bird of paradise feather coloration and their vision similarly indicates coordination of their mating displays with spectral properties through the avian visual system (Wilts, Michielsen et al. 2014). Individual birds actively control the signaling functions of their feathers with feathers or ornaments hidden/displayed or even the color presented (as dark/black vs. vibrant/iridescent) being consciously restricted or directed to particular

viewers such as potential mates or rivals (Wilts, Michielsen et al. 2014).

Fossilized feathers typically have been evaluated within two-dimensional surface views, limiting the understanding of their overall ultrastructure and perhaps their true coloration. As a step forward in our reconstruction of the structure and function (color display) of early bird feathers, we examined the unique head-crest feathers of a well-preserved specimen (Institute of Vertebrate Paleontology and Paleoanthropology, IVPP V26899) of the Early Cretaceous (~120 Ma) enantiornithine *Shangyang* sp. from the Jiufotang Formation of northeastern China. This fossil preserves a diverse feather assemblage across the body with dense contour feathers, flight remiges, and two rachis-dominated tail feathers (Figure 1 and figure S1). Among its diverse feather morphologies, this specimen also displays a strikingly enlarged feathered crest on the head that uniquely extends from the caudal end of the skull to a position rostral to the nasal bone (Figure 1). For our study, we sampled a long isolated mature feather that is displaced from the caudal part of the crest, as well as three feather fragments extracted from the *in-situ* position of the head crest.

In this study, we utilized serial ultrathin histological sectioning, scanning/transmission electron microscopy (S/TEM) imaging, and finite-difference time-domain (FDTD) modeling to investigate the potential iridescent coloration mechanisms in the elongated crest feathers from this newly discovered enantiornithine specimen of the Jehol Biota. Differing from previous statistical reconstructions of fossil color that measured melanosome aspect

ratios, our new approach takes the three-dimensional shape and packing patterns of melanosomes, as well as the keratinous matrix, into consideration. With these novel modeling approaches, a more accurate coloration estimation was produced for its crest feather.

Results

In the new fossil, head crest feathers were selected from the caudal side of the head and sectioned using ultrathin serial sectioning. The overall shape of the sampled crest feather is well-preserved and comprised of elongate and relatively wide barbs. The dominant barb length is proportionally longer than the feather barb examined from the neck and head region of *Confuciusornis* (Foth 2012). The feather is different from the bilaterally symmetric plumulaceous feathers of living birds, and we define it as a barb-dominant feather, since most of the exposed feather tissue is composed of long barbs with a very short and thick calamus. It is estimated to correlate with evolutionary stage II and IIIa of (Prum and Brush 2002), similar to the intermediate feather type proposed as found in an amber fossil (Perrichot, Marion et al. 2008). The new feather described here is distinct from the amber feather in showing an asymmetric shape, radically diverging toward one side (caudal side), and is much larger in size (Perrichot, Marion et al. 2008). There are dense clusters inside the barbs as seen from images of both SEM and TEM.

Ultrathin histological sectioning and application of SEM and S/TEM imaging of the fossil feather samples (see Supplementary materials) resulted in the identification of partially

132 interlinked melanosomes with a derived asymmetric packing pattern (Figures 2 and 3).
133 The long axial crack in Figure 2 may represent the surface of the barbs, resembling a
134 crack formed in maturation experiments (Zhao, Hu et al. 2020). Those melanosome
135 clusters are present and concentrated mostly within the barbs rather than in the barbules
136 of extant bird feathers based on similar size (Figure 2). The long axis of the densely
137 packed melanosomes is aligned overall parallel with the barb's long axis (Figure 2), which
138 has been confirmed by detailed histological data as well. The melanosomes are arranged
139 in an asymmetric hexagonal conformation, clearly visible in the different sections (see
140 Figure 3).
141
142 SEM imaging of the cross section and surface view of the sampled feather indicate the
143 presence of a few major barbs without barbules (figures S1 and S3-4). The thickness of
144 the complete feather barb with filled melanosomes (preserved) is around 10 μm, which is
145 much greater than the typical diameter of known barbules, but similar to barbs in extant
146 birds (Freyer, Wilts et al. 2021). The three-dimensionally packed melanosomes were
147 studied in both cross and nearly longitudinal sections within the dark colored barbs (one in
148 the middle of the barbs and another in the lateral side of the feather block (Figure 3a, b).
149
150 Hooks are commonly observed on the oval-shaped melanosomes in cross-sectional
151 views, with two dominant types identified on the dorsal and ventral sides (Figure 3c-d, red
152 arrows). These hooks are deflected in opposing directions, linking melanosomes from
153 different arrays (dorsal-ventral) together. The major axis(y) of the oval-shaped

154 melanosomes (mean = 283 nm) is oriented toward the left side in cross-section, while the
155 shorter axis(x) measures approximately 186 nm (Table S2). In oblique or near-longitudinal
156 sections (Figure 3e-f), the hooked structures' connections to the distal and proximal sides
157 of neighboring melanosomes are clearly visible (blue arrows, Figure 3f). The mean long
158 axis (z) of the melanosomes is approximately 1774 nm (Table S2). A similar pattern
159 occurs in two additional regions of interest within the same feather (figure S5). Although
160 the smaller proximal hooks in these sections are less distinct, this may reflect
161 developmental variation during melanosome formation along the feather barb.
162 Significantly smaller hooks were also observed in cross-sections of *in-situ* feather barbs
163 from the anterior side of the feather crest (figure S6). Based on these observations, we
164 propose that the hooked structures—particularly those on the dorsal, ventral, proximal,
165 and distal sides of the melanosomes—enhance the structural integrity of the barb (figure
166 S7). However, these features may be teratological and unique to this individual, as no
167 similar structures have been reported in other species. These hooks may stabilize the
168 stacked melanosome rods and contribute to increased barb dimensions, such as diameter
169 and length. The sections exhibit modified (or asymmetric) hexagonally packed
170 melanosomes with presence of extra hooked linkages (Figure 3c-d and e-f). The long
171 rod-like melanosomes are different from all other known feather melanosomes from both
172 extant and extinct taxa in having some extra hooks and an oblique ellipse shape in cross
173 and longitudinal sections of individual melanosomes (Durrer 1986, Zhang, Kearns et al.
174 2010). The asymmetric packing of the melanosomes (the major axis leans leftward in
175 cross section) played a major role in the reduction of fossilized keratinous matrix within

the barbs, which may correspond to a novel structural coloration in this extinct bird. The close packed hexagonal melanosome pattern found in extant avian feathers yield rounded melanosome outlines in contrast to the oval-shaped melanosomes (see figure S8, x<y) in the perpendicular section here. The asymmetric compact hexagonal packing (ACHP) of the melanosomes is different from the known pattern of melanosomes formed in the structure of barbules among extant birds (Eliason and Shawkey 2012), which has been seen as a regular hexagonal organization. The packing of the melanosomes in an asymmetric pattern, on the microscopic level, might be related to the asymmetrical path of the barb extension direction observed at the macroscopic level (figure S5).

In the computational (FDTD) simulation, when light is incident at a small angle (≤30°, both s- and p-polarized) in the X-Y plane, no evident reflection peak was found in the visible spectrum, as shown in Figure 4c (e.g., when a viewer observes at this angle, the light is almost completely absorbed, and the crest feather would have a darkened appearance). As the incident angle varies from 40° to 70°, the wavelength corresponding to the reflection peak shifts from 687 nm to 475 nm, and the color of the reflection peak gradually changes from red to deep blue (inset in Figure 4c clearly shows how the resulting color varies with the angle of incidence). From the perspective of optical modeling, the generation of iridescent color (reflection peaks in the visible spectrum) is caused by the constructive interference between scattered light produced by these uniquely shaped melanosomes that are compactly arranged in the barbs (Vinther, Briggs et al. 2010). Between blue and red, reflection peaks of green and yellow also are present,

198 corresponding to the wavelengths of 512 nm and 578 nm respectively. It is worth noting
199 that in the case of both p- and s-polarized incident light, the positions of the reflection
200 peaks are nearly identical, with only a slight difference in peak reflectance. Therefore, the
201 three-dimensional multilayer nanostructure model is somehow equivalent to
202 one-dimensional multilayer biphotonic crystals (Saranathan, Forster et al. 2012). In
203 summary, the crest feather of the Cretaceous enantiornithine shows a strikingly
204 angle-dependent and iridescent coloration pattern. When we consider the shrinkage effect
205 on melanosomes demonstrated experimentally (McNamara, Briggs et al. 2013) and
206 various distances between melanosomes resulting from compression effects (Pan et al.
207 2019; Zhao et al. 2020), our additional FDTD modeling shows a similar reflection
208 spectrum with a narrower bandwidth of the color peaks (Supplemental Materials).
209

210 ## Discussion

211 This study of a fossilized feather with a combination of microscopic imaging, ultrathin
212 sectioning, and three-dimensional modeling has provided a more accurate examination of
213 ancient structural coloration and uncovered unusual melanosome structures. Using
214 previous conventional approaches alone, we would have classified this feather crest
215 simply as black or close to iridescent based on its melanosome aspect ratio (Nordén,
216 Eliason et al. 2021). The recognition of overall iridescence links to a commonly found
217 extant bird color range only known previously from the platelet-shaped dinosaurian
218 melanosomes (Hu, Clarke et al. 2018) and a few fossil feathers (Pan, Li et al. 2022)
219 (Nordén, Faber et al. 2019, Nordén, Eliason et al. 2021). The independent evolution of

220 overall iridescence, similar to that found in living birds, was reconstructed here based on a
221 novel array of melanosomes in a feather barb in an extinct non-crown group bird (Nordén,
222 Faber et al. 2019, Yoshioka and Akiyama 2021). The occurrence of iridescent structural
223 coloration in an enlarged head crest on this ancient bird is similar to structures present
224 across many living birds that employ iridescence for intimidation, signaling, and
225 particularly for mate attraction or intraspecific territorial defense (Terrill and Shultz 2023).
226 Given that this individual bird likely was a male based on the occurrence of paired rachis
227 dominant tail feathers (figure S1), the vibrant coloration on a prominent feathered crest
228 suggests that sexual selection may have long played an important role in avialan (feather)
229 macroevolution (Foth 2020, Wang, O'Connor et al. 2021). The vibrant color and its
230 presence on an enlarged feather crest likely are interlinked, and probably indicate an
231 evolutionary and selective relationship among color, feather position, and feather
232 morphology/size.
233
234 Our discovery of new melanosome shapes and networks suggests that birds evolved
235 previously unrecognized patterns of color production outside of the limits present among
236 crown group birds. Additionally, these pigments and their dense organization may have
237 made the foundation of the feather darker and allowed for a more intense or vibrant
238 iridescent coloration, a potential relationship that is understudied among living birds. While
239 the interrelationship between melanin content in feathers and increases in structural
240 strength have long been known (Burtt 1981, Burtt Jr and Ichida 2004), perhaps the
241 increased density of melanosomes in this fossil feather barbs added even more structural

242 strength to the feathered crest of this bird in compromise for its lack of a dominant rachis.
243 Additionally, the interlocking hooks among the melanosomes might have aided individual
244 feather barb in resisting shear forces. The modified closely packed melanosome arrays
245 reconstructed here also are potentially advantageous in increasing barb structural
246 integrity and stability in the long barb ramus, and likely affected the visualized spectrum
247 during the display of iridescent coloration. We cannot completely rule out the increased
248 melanosome density in the fossil feather is the result of taphonomy. Size reduction in
249 melanosomes was found previously in a simulation experiment (McNamara, Briggs et al.
250 2013), but such a reduction is very unlikely to result in the highly organized and consistent
251 melanosome packing present here (McNamara, Briggs et al. 2013, Zhao, Hu et al. 2020).
252 To test the potential impact of melanosome shrinkage and potential taphonomic changes
253 to their spacing, we conducted an additional analysis (See Supplementary Materials), and
254 the results yield similar iridescent spectral peaks as the original setting.
255
256 Since the iridescent coloration of living birds is produced by the accumulation of
257 melanosomes mostly positioned in barbules, the identified fossil barbs filled with
258 melanosomes represents a unique phenotype related to an early feather evolutionary and
259 developmental stage. Given the lack of barbules in most early primitive feather forms (or
260 filamentary structures) in non-avialan dinosaurs and pterosaurs, the positioning of
261 melanosomes in barbs might be a plesiomorphic feature for ornithodirans broadly (Xu
262 2019, Cincotta, Nicolaï et al. 2022). With different destinations of melanosome transport
263 during feather formation, the pattern recovered here suggests fundamental differences in

264 feather pigmentation among Cretaceous stem taxa as compared to crown birds. The
265 melanosome-filled barbs evolved earlier in feather evolution before the later appearance
266 of innovations such as the presence of a stiff rachis and colorful barbules observed across
267 living feathers (Yu, Wu et al. 2002).
268
269 A focus on the two-dimensional examination of fossil feathers has uncovered a large
270 number of black or dark melanosomes across many early birds and feathered theropods
271 (Li, Clarke et al. 2014, Hu, Clarke et al. 2018). However, our three-dimensional study of a
272 fossilized Jehol feather specimen demonstrates that ultra-histological detail and spatial
273 relationships can be preserved at the microscopic level. Importantly, our discovery
274 suggests that reexamination of previously published 'black' pigmented fossil feathers
275 might uncover a wider occurrence of 'surprising' iridescence and structural coloration
276 among these early birds and non-avialan taxa. Such discoveries will aid in documenting
277 both independent and convergent evolutionary pathways in the history of birds. This
278 research further demonstrates that Jehol fossil feather tissue can be treated as
279 (microscopically) three dimensional specimens allowing for the collection of valuable
280 comparative data and application of comparative analytical techniques that facilitate a
281 better understanding of early feather evolution and function.
282
283 Here, we recovered iridescent coloration in fossil bird feathers that was produced by
284 three-dimensional melanosome packing patterns. This discovery dramatically expands
285 the range of fossil bird coloration space, and this diversity in feather coloration in an early

286 bird fits well with its forested environment, as proposed by the coeval fossil plant
287 community (Wu, Li et al. 2023). Tropical forest environments are accompanied by colorful
288 flowing plants and green leaves, and the structural color of this feathered crest is
289 advantageous for bird signaling as well. Forested environments (flowers, leaves, light, and
290 shadow) can be advantageous for birds and their signaling as more colorful feathers are
291 found today in tropical regions as demonstrated among extant vibrant coloration of
292 passeriform birds in particular (Cooney, He et al. 2022).
293

294 ## Materials and Methods

295 ### Fossil material

296 The referred specimen of the enantiornithine bird *Shangyang* sp. (IVPP V 26899) was
297 recovered near La-Ma-Dong Village in Jian-Chang County, within the Jiufotang Formation
298 (dated ~120 Ma). It can be referred to *Shangyang* by the presence of derived features in
299 the premaxillae, tibiotarsus, and sternum (Figure 1 and Supplementary Materials).
300

301 The feather fragment (labeled sample Figure 1) extracted from the specimen were mainly
302 analyzed using SEM (Scanning Electron Microscopy) and S/TEM
303 (Scanning/Transmission Electron Microscopy). The extracted feather sample is one of the
304 longest crest feathers, was displaced far from the caudal position of the skull (sample in
305 Figure 1), and belongs to a fully mature asymmetric barb dominant feather. In addition to
306 the singular feather, three fragments of other feathers were extracted from the *in-situ*
307 position of the head crest and sampled to validate the revealed structure (Supplementary

308 Materials, figure S6). A small fragment of the right femur was extracted to produce a
309 ground-section to evaluate osteo-histological features in relation to its ontogenetic stage
310 (figures S1 and S2).
311

312 ## Scanning electron microscopy (SEM)

313 Feather samples coated with gold were examined with a FEI ESEM Quanta 450, which is
314 operated at the Tectonic Laboratory in the China Geological Survey in Beijing, China. The
315 SEM was operated with about 10 mm working distance of the sample under a high voltage
316 of 20 KV. Not only the surface of feather sample was examined, but the raw material of
317 the cross-section exposed in the ultrathin sliced sections also were imaged to
318 characterize an overall distribution and thickness of soft tissue in comparison with the
319 adjacent sediment or matrix (Figure 2 and figures S3). Additionally, a FIB-SEM (Heliox
320 5CX Due Beam system) also was further applied to validate the melanosome packing in
321 an extracted volume, and the imaged block is about 11 x 13 x 9μm (figure S7).

322 ## Scanning/Transmission Electron Microscopy

323 The crest feather fragments were embedded in epoxy resin using the SPI-PON 812
324 Embedding Kit (MNA, EPOK, DDSA, DMP-30)(Luft 1961) at the Key Laboratory of
325 Vertebrate Evolution and Human Origins of the Chinese Academy of Sciences in Beijing
326 in 2022. After a step-wised polymerization at 37°C for 12 hours, 45°C for 12 hours, and
327 60°C for 48 hours, the epoxy-embedded block was prepared and cut using an ultrathin
328 slicing machine (Lecia EM UC7), equipped with a diamond knife (ultra 45°, 3 mm) for
329 further TEM observations. The ultrathin slices were placed on copper grids with carbon

330 film (200 meshes in ~3 mm diameter copper gird). The thickness of a prepared ultrathin
331 slice is approximately ~70 nm, and the slices were consecutively placed on ~3-5 copper
332 grids. The removed thickness of the sample for making those ~3-5 copper grids for one
333 run of sectioning (serial numbered grids were made) took about ~20 μm of the prepared
334 pyramidal-cubic shaped block (Figures 3 and 5). The direction of slicing was either
335 perpendicular to the long axis of the barbs, or nearly parallel with the long axis of the barb,
336 for the two spots selected for cutting.
337
338 S/TEM imaging was conducted on a Thermo Scientific (FEI) Talos F200X G2 TEM at the
339 IVPP, Beijing during 2021-2022. The Talos F200X was operated at 200 KV with an
340 analytical scanning transmission electron microscope mode (S/TEM). TEM slices were
341 made from the isolated feather adjacent to the head and rostral portion of the skull. The
342 two specific micron-sized spots of the feather were targeted for examination of their
343 microscopic features by ultrathin slicing and examination as shown in Figure 3. For the
344 long contour feather, one spot close to the middle of the feather was made as a cross
345 section of the barb, and for the other spot, the slice was made close to the left side of the
346 fragment with a longitudinal slice (Figure 3). The strategic consideration of the two
347 directions (and spots) of cutting was to examine the melanosomes and other features in
348 different views in order to visualize these different features and obtain three-dimensional
349 data (see Supplementary Materials).
350
351 **X-ray computed tomography**

352 The fossil slab was scanned using a GE |phenix| micro-scanner with a resolution of 24.3
353 μm at Key Laboratory of Vertebrate Evolution and Human Origins, IVPP, Chinese
354 Academy of Sciences, Beijing. For the skeletal anatomy of the bird, μ-CT scans and digital
355 rendering were applied to aid in visualizing the skeletal features of the new specimen
356 (Figure 1). The digital rendering of the specimen was completed using Avizo 9.0. (Figure
357 1). Measurements were made using digital calipers, as well as validated in the CT data
358 digitally (Table S1). To achieve optimized image resolution, the field of view was adjusted,
359 resulting in part of the feet being excluded from the CT scan.
360

361 ## Technical protocol for ultrathin slicing

362 Prior to the work presented here, we obtained numerous practice sections from a few
363 samples of fossil feathers. In our prior samples, the fragmentary feather tissues were used
364 to improve the technician's capability and precision in sectioning exercises by comparison
365 with the desired direction and sectioned direction for given a fossil. There are several key
366 steps elaborated below for the successful repetition of practices of sectioning in the
367 correct alignment. First, we examined the fossil feathers with light microscopy and SEM
368 prior to the embedding process to make sure the barbs were aligned correctly in the epoxy
369 resin. Meanwhile, the small part of the extracted feather sample was aligned, using the
370 microscope (Lecia UC 7), into a proper position during the emending and stage trimming
371 process. The attention to feather direction was performed to assure that the barb major
372 extension direction was aligned with the long axis of the bullet mold (embedding capsule).
373 We also checked the position of the feather fragment in the SPI-Pon 812 during

374 embedding and polymerization. The sliced section should be precise enough to acquire
375 the desired images and information after planning and optimization of each step described
376 above, and before the sectioning. Of course, the ultrathin slicing practices can improve the
377 technician's skill and increase cutting precision which require a gradual learning process.
378
379 **FDTD modeling of the feather's reflectance**
380 To explore the coloration of the three-dimensionally packed melanosomes, Lumerical
381 finite-difference-time-domain (FDTD) software (Ansys Canada Ltd.) (Inan and Marshall
382 2011, Sullivan 2013) was used to simulate the visualization of light propagation on the
383 crest feather with regular arrangements of melanosomes (Figure 1). The FDTD method
384 allows explicit simulation of light interaction with particular-shaped melanosomes by
385 numerically solving Maxwell's equation in the time domain. The construction of a
386 three-dimensional nanostructure model is based on our characterized data (Figure 4 and
387 Table S2), and detailed modeling steps are included in Supplementary Materials. The
388 dispersion of the complex refractive index that was applied in our simulation is described
389 and shown in figure S9. In order to mimic real visual conditions, several variables were
390 considered during the simulation, including angle of light incidence in two orthogonal
391 incident planes (X-Y and Y-Z plane) (Figure 4b) and polarization state (s- and p-polarized).
392 Usually, p-polarized light is understood to have an electric field direction parallel to the
393 plane of incidence, and s-polarized light has the electric field oriented perpendicular to the
394 incident plane. Reflectance spectra are presented in Figure 4c-d.
395

Caveats about potential taphonomic melanosome changes

The simulated colors here are robust even when taking potential taphonomic changes into consideration. The chance that the highly organized and anatomically oriented nanoscale pattern formed here is the result of geological compression or pressure during fossilization and diagenesis is quite low, and such structures are absent or unseen among known taphonomic artifacts (McNamara, Briggs et al. 2013, Zhao, Hu et al. 2020). At present, we cannot exclude the possibility that sheer stress could result in the observed asymmetric packing of melanosomes. However, that pattern has not been reported in any known experiment or geological process of fossilization including those related to Jehol bird or non-avialan dinosaur fossils. Therefore, we suggest the pattern we obtained here represents original biological structures. Given experimental observations of melanosome shrinkage at high pressures and temperatures (~10% shrinkage) (McNamara, Briggs et al. 2013, Zhao, Hu et al. 2020), we also completed additional modeling with the fossil melanosomes enlarged (110%, see Table S3) along with the fossilized keratinous cortex and matrix. This additional modeling resulted in all of the spectral peaks present in the original modeling being recovered. Therefore, our results are robust even when considering known potential taphonomic artifacts, and both approaches produce similar results with the red-to-blue iridescent coloration having been present in the crown feather (figure S10).

References

Benton, M. J., D. Dhouailly, B. Jiang and M. McNamara (2019). "The early origin of feathers." Trends in ecology & evolution **34**(9): 856-869.

Burtt, E. H., Jr. (1981). "The Adaptiveness of Animal Colors." BioScience **31**(10): 723-729.

Burtt Jr, E. H. and J. M. Ichida (2004). "Gloger's rule, feather-degrading bacteria, and color variation among song sparrows." The Condor **106**(3): 681-686.

Cincotta, A., M. Nicolaï, H. B. N. Campos, M. McNamara, L. D'Alba, M. D. Shawkey, E.-E. Kischlat, J. Yans, R. Carleer, F. Escuillié and P. Godefroit (2022). "Pterosaur melanosomes support signalling functions for early feathers." Nature **604**(7907): 684-688.

Cooney, C. R., Y. He, Z. K. Varley, L. O. Nouri, C. J. Moody, M. D. Jardine, A. Liker, T. Székely and G. H. Thomas (2022). "Latitudinal gradients in avian colourfulness." Nature Ecology & Evolution **6**(5): 622-629.

Durrer, H. (1986). "Colouration." Biology of the integument: 2 vertebrates: 239-247.

Eliason, C. M. and M. D. Shawkey (2012). "A photonic heterostructure produces diverse iridescent colours in duck wing patches." Journal of The Royal Society Interface **9**(74): 2279-2289.

Foth, C. (2012). "On the identification of feather structures in stem-line representatives of birds: evidence from fossils and actuopalaeontology." Paläontologische Zeitschrift **86**(1): 91-102.

Foth, C. (2020). "A morphological review of the enigmatic elongated tail feathers of stem birds." The evolution of feathers: from their origin to the present: 173-184.

Foth, C. and O. W. Rauhut (2020). "The evolution of feathers." From Their Origin to the Present. Cham: Springer.

Freyer, P., B. D. Wilts and D. G. Stavenga (2021). "Cortex thickness is key for the colors of iridescent starling feather barbules with a single, organized melanosome layer." Frontiers in Ecology and Evolution **9**: 746254.

Hu, D., J. A. Clarke, C. M. Eliason, R. Qiu, Q. Li, M. D. Shawkey, C. Zhao, L. D'Alba, J. Jiang and X. Xu (2018). "A bony-crested Jurassic dinosaur with evidence of iridescent plumage highlights complexity in early paravian evolution." Nature Communications **9**(1): 217.

Inan, U. S. and R. A. Marshall (2011). Numerical electromagnetics: the FDTD method, Cambridge University Press.

Li, Q., J. A. Clarke, K.-Q. Gao, C.-F. Zhou, Q. Meng, D. Li, L. D'Alba and M. D. Shawkey (2014). "Melanosome evolution indicates a key physiological shift within feathered dinosaurs." Nature **507**(7492): 350-353.

Li, Q., K.-Q. Gao, Q. Meng, J. A. Clarke, M. D. Shawkey, L. D'Alba, R. Pei, M. Ellison, M. A. Norell and J. Vinther (2012). "Reconstruction of *Microraptor* and the evolution of iridescent plumage." Science **335**(6073): 1215-1219.

Li, Q., K.-Q. Gao, J. Vinther, M. D. Shawkey, J. A. Clarke, L. D'Alba, Q. Meng, D. E. Briggs and R. O. Prum (2010). "Plumage color patterns of an extinct dinosaur." science **327**(5971): 1369-1372.

Luft, J. H. (1961). "Improvements in epoxy resin embedding methods." The Journal of Cell Biology **9**(2): 409-414.

McNamara, M. E., D. E. Briggs, P. J. Orr, D. J. Field and Z. Wang (2013). "Experimental maturation of feathers: implications for reconstructions of fossil feather colour." Biology Letters **9**(3): 20130184.

Nordén, K. K., C. M. Eliason and M. C. Stoddard (2021). "Evolution of brilliant iridescent feather nanostructures." eLife **10**: e71179.

Nordén, K. K., J. W. Faber, F. Babarović, T. L. Stubbs, T. Selly, J. D. Schiffbauer, P. Peharec Štefanić, G. Mayr, F. M. Smithwick and J. Vinther (2019). "Melanosome diversity and convergence in the evolution of iridescent avian feathers — Implications for paleocolor reconstruction." Evolution **73**(1): 15-27.

Pan, Y., Z. Li, M. Wang, T. Zhao, X. Wang and X. Zheng (2022). "Unambiguous evidence of brilliant iridescent feather color from hollow melanosomes in an Early Cretaceous bird." National Science Review **9**(2): nwab227.

Perrichot, V., L. Marion, D. Néraudeau, R. Vullo and P. Tafforeau (2008). "The early evolution of feathers: fossil evidence from Cretaceous amber of France." Proceedings of the Royal Society of London B: Biological Sciences **275**(1639): 1197-1202.

Peteya, J. A., J. A. Clarke, Q. Li, K. Q. Gao and M. D. Shawkey (2017). "The plumage and colouration of an enantiornithine bird from the Early Cretaceous of China." Palaeontology **60**(1): 55-71.

Prum, R. (2006). "Bird Coloration, Vol. 1, Mechanisms and Measurements."

Prum, R. O. and A. H. Brush (2002). "The evolutionary origin and diversification of feathers." The Quarterly review of biology **77**(3): 261-295.

Saranathan, V., J. D. Forster, H. Noh, S. F. Liew, S. G. Mochrie, H. Cao, E. R. Dufresne and R. O. Prum (2012). "Structure and optical function of amorphous photonic nanostructures from avian feather barbs: a comparative small angle X-ray scattering (SAXS) analysis of 230 bird species." J R Soc Interface **9**(75): 2563-2580.

Stoddard, M. C., H. N. Eyster, B. G. Hogan, D. H. Morris, E. R. Soucy and D. W. Inouye (2020). "Wild hummingbirds discriminate nonspectral colors." Proceedings of the National Academy of Sciences **117**(26): 15112-15122.

Stoddard, M. C. and R. O. Prum (2011). "How colorful are birds? Evolution of the avian plumage color gamut." Behavioral Ecology **22**(5): 1042-1052.

Sullivan, D. M. (2013). Electromagnetic simulation using the FDTD method, John Wiley & Sons.

Terrill, R. S. and A. J. Shultz (2023). "Feather function and the evolution of birds." Biological Reviews **98**(2): 540-566.

Vinther, J., D. E. Briggs, J. Clarke, G. Mayr and R. O. Prum (2010). "Structural coloration in a fossil feather." Biol Lett **6**(1): 128-131.

Vinther, J., D. E. Briggs, R. O. Prum and V. Saranathan (2008). "The colour of fossil feathers." Biology Letters **4**(5): 522-525.

Wang, M., J. K. O'Connor, T. Zhao, Y. Pan, X. Zheng, X. Wang and Z. Zhou (2021). "An Early Cretaceous enantiornithine bird with a pintail." Current Biology **31**(21): 4845-4852.e4842.

Wilts, B. D., K. Michielsen, H. De Raedt and D. G. Stavenga (2014). "Sparkling feather reflections of a bird-of-paradise explained by finite-difference time-domain modeling." Proceedings of the National Academy of Sciences **111**(12): 4363-4368.

Wu, Y., Z. Li, T. A. Stidham and S. Y. Foong (2023). "Phytolith evidence reveals the origin of angiosperm leaf eating habits among ancient Cretaceous birds." The Innovation **4**(5).

Xu, X. (2019). "Feather evolution: looking up close and through deep time." Sci Bull (Beijing) **64**(9): 563-564.

Yoshioka, S. and T. Akiyama (2021). Mechanisms of Feather Structural Coloration and Pattern Formation in Birds. Pigments, Pigment Cells and Pigment Patterns. H. Hashimoto, M. Goda, R. Futahashi, R. Kelsh and T. Akiyama. Singapore, Springer Singapore: 343-366.

Yu, M., P. Wu, R. B. Widelitz and C.-M. Chuong (2002). "The morphogenesis of feathers." Nature **420**(6913): 308-312.

Zhang, F., S. L. Kearns, P. J. Orr, M. J. Benton, Z. Zhou, D. Johnson, X. Xu and X. Wang (2010). "Fossilized melanosomes and the colour of Cretaceous dinosaurs and birds." Nature **463**(7284): 1075-1078.

Zhao, T., J. Hu, L. Hu and Y. Pan (2020). "Experimental maturation of feathers: implications for interpretations of fossil feathers." Palaios **35**(2): 67-76.

Zi, J., X. Yu, Y. Li, X. Hu, C. Xu, X. Wang, X. Liu and R. Fu (2003). "Coloration strategies in peacock feathers." Proceedings of the National Academy of Sciences **100**(22): 12576-12578.

Acknowledgments

We thank: Yang JM, Ma JB, Wen XL, and Li DS for technical assistance in sampling and ultrathin sectioning and STEM imaging; Hou YM and Yin PF for assistance with micro-CT scanning of the specimen; Gao W for photography; and Xu Y for the artistic reconstruction. Two reviewers are grateful in providing valuable suggestions for improving earlier version of the manuscript.

Funding:

National Natural Science Foundation of China 42288201(ZZ), National Key Research and Development Project of China (2024YFF0807603) (ZL) and (2024YFF0807602) (YP); NSFC 42472047 (ZL), 37110101 (MY), and NSFC Fund for Excellent Young Scholars KZ 37110101 (MY).

Author contributions:

Conceptualization: ZL and ZZ

Methodology: JH, MY and ZL

Investigation: ZL, TAS, JH, YM, and JAC

Visualization: JH and ZL

Supervision: ZL and ZZ

Writing—original draft: TAS, ZL, YP, MW, JL and TZ

Writing—review & editing: ZL, JH, TAS, MY, MW, YP, TZ, JL, ZZ, and JAC

Competing interests: All other authors declare they have no competing interests.

Data and materials availability: All data are available in the main text or the supplementary materials

Figures Legends

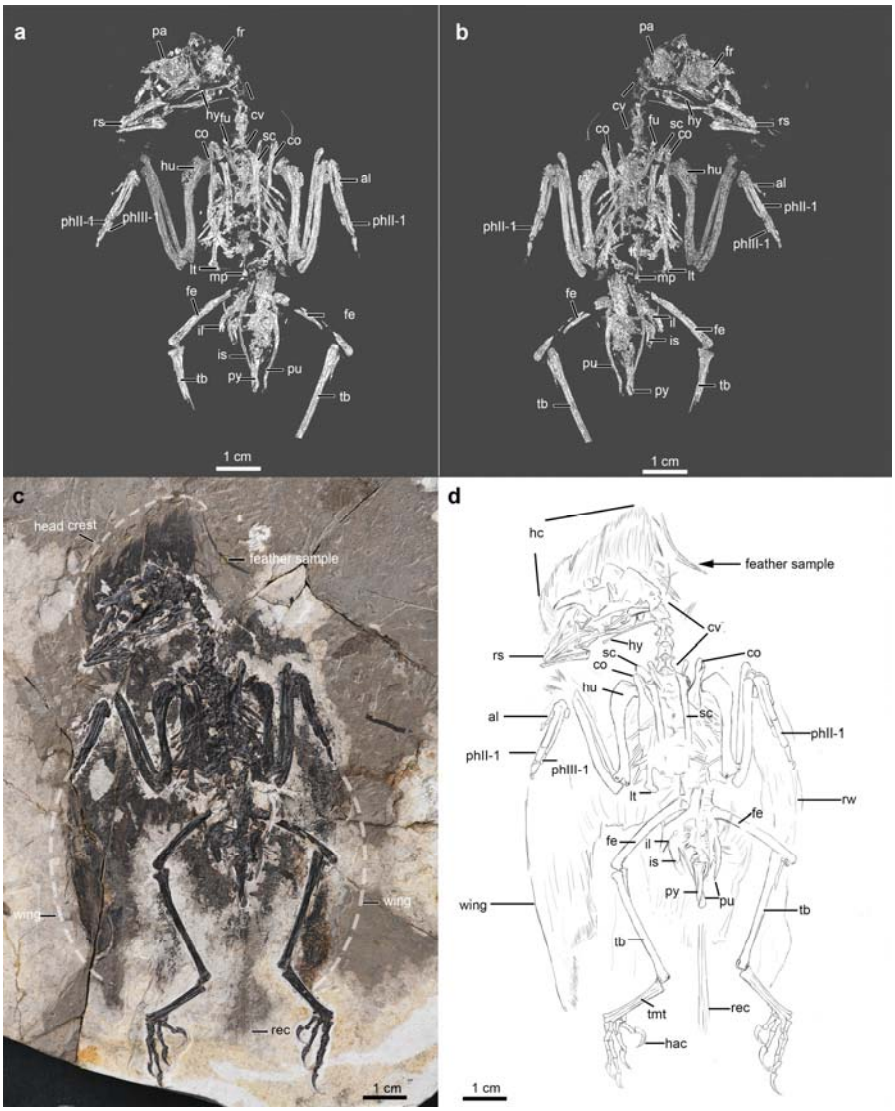

Figure 1 Digital rendering, photography, and line-drawing of the enantiornithine fossil specimen (*Shanyang* sp., IVPP V26899) (a), (c), (d) - dorsal; (b)- ventral view showing the major skeletal elements. The feather extracted from the crown are labeled as feather sample (**c**). Abbreviations: al, alular metacarpal; co, coracoid; cv, cervical vertebra; fe, femur; fi, fibula; fr frontal; fu, furcula; hac, hallucal ungual; hc, head crest; hu, humerus; hy, hyoid; il, ilium; is, ischium; lt, lateral trabecula; mcf, molted crest feather; mc II, major metacarpal; mp, midline process; ph II-1, first digit of phalanx II; phIII-1, first digit of

phalanx III; pa, parietal; pu, pubis; py, pygostyle; r, radius; rec, rectrices; rem, remiges; rs, rostrum; rw, right wing; sc, scapula; sk, skull; st, sternum; tb, tibiotarsus; and tmt, tarsometatarsus.

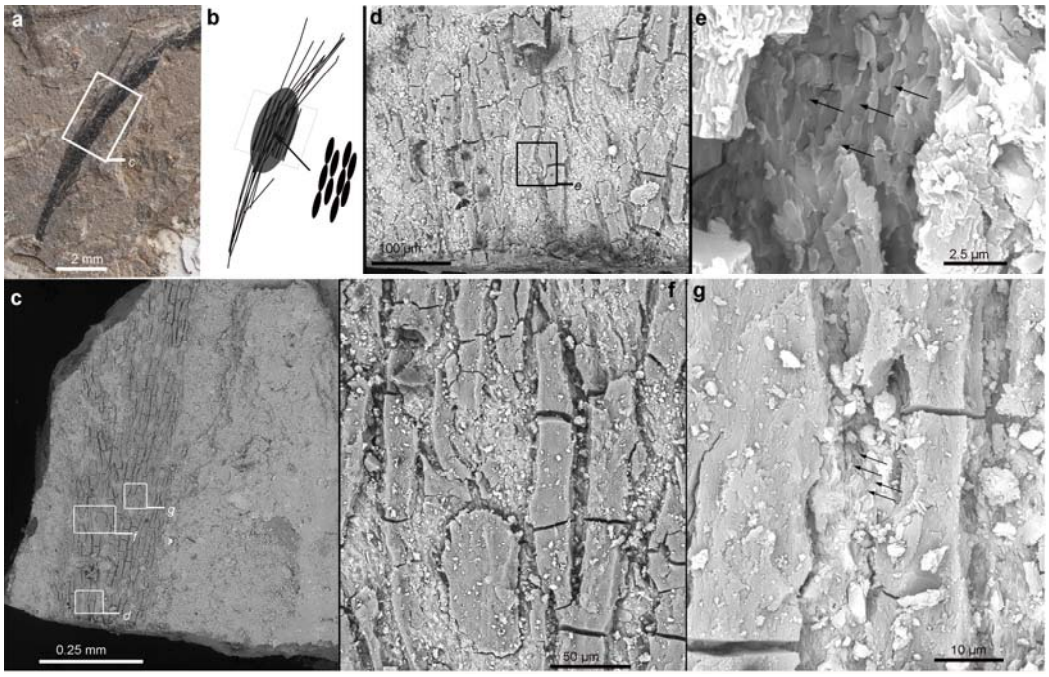

Figure 2 Photograph (a) and simplified line-diagram (b) of the sampled isolated long feather with a focused area from SEM imaging (c-g). As shown in the SEM images, the long elliptical or oval-shaped melanosomes are tightly aligned with their long axis parallel to the elongated barbs (**e, g**). The position of enlarged images (**d, e, f, and g**) is indicated as square in (**c, d**); black arrows in (**e**) and (**g**) indicate the melanosome clusters.

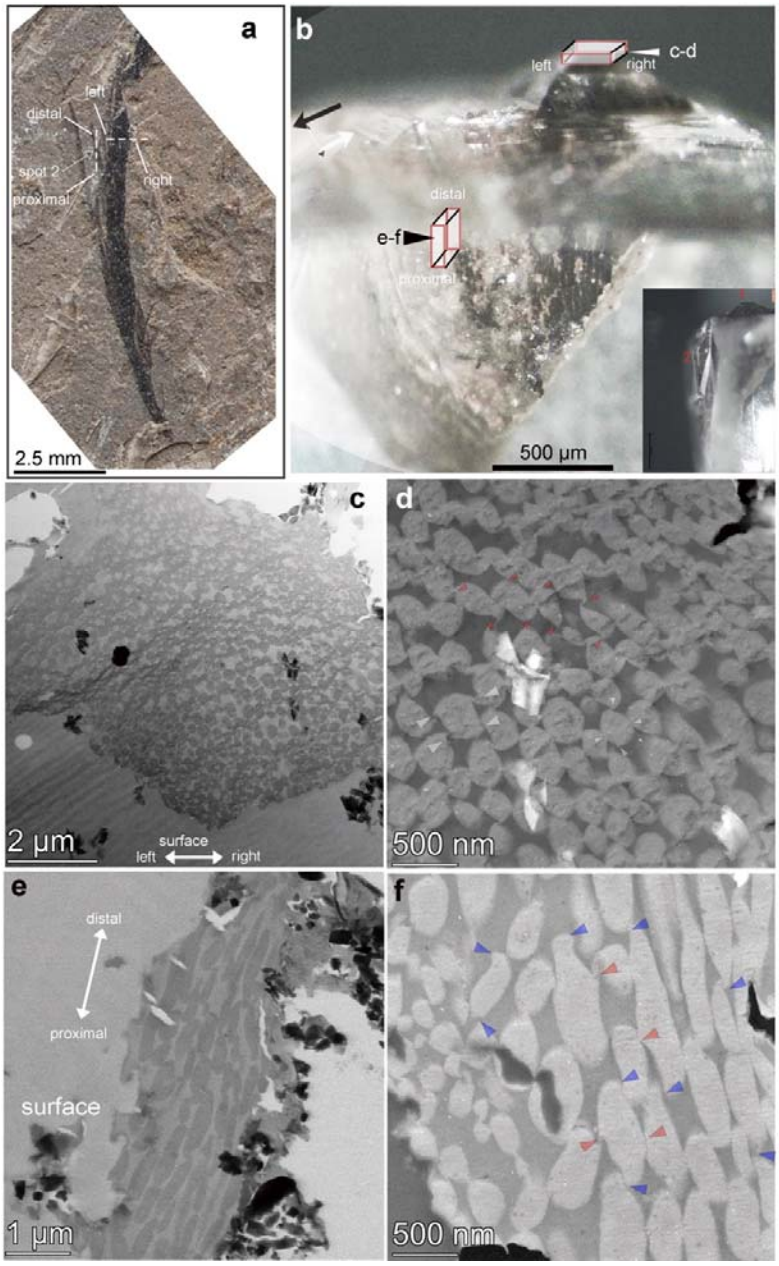

Figure 3. Photograph of the crest feather (a) and prepared blocks of the feather barb (b) for thin sectioning. The sampled spots for the sliced feather are indicated as long red-colored cubes with their respective positions in (**b**). (**c**) to (**f**) are (STEM) images obtained from individual slices as indicated in (**b**). The shape and arrangement of the melanosome packing (ACHP, asymmetric compact hexagonal packing) is clearly revealed in (**d**); (**c**) and (**d**) are derived from the cross-section; (**e**) and (**f**) are derived from the nearly

longitudinal section. As indicated by the red arrows in (d) and (f), the dorsal and ventral hooks are dominant in the cross-sectional images. On the other hand, hooks connecting the proximal and distal arrays of melanosomes are better visualized in the longitudinal section, as labeled with blue arrows in (f). Orientation of the slices were labeled (left, right, proximal, distal) with their respective petitioning in the fossil before and during sectioning.

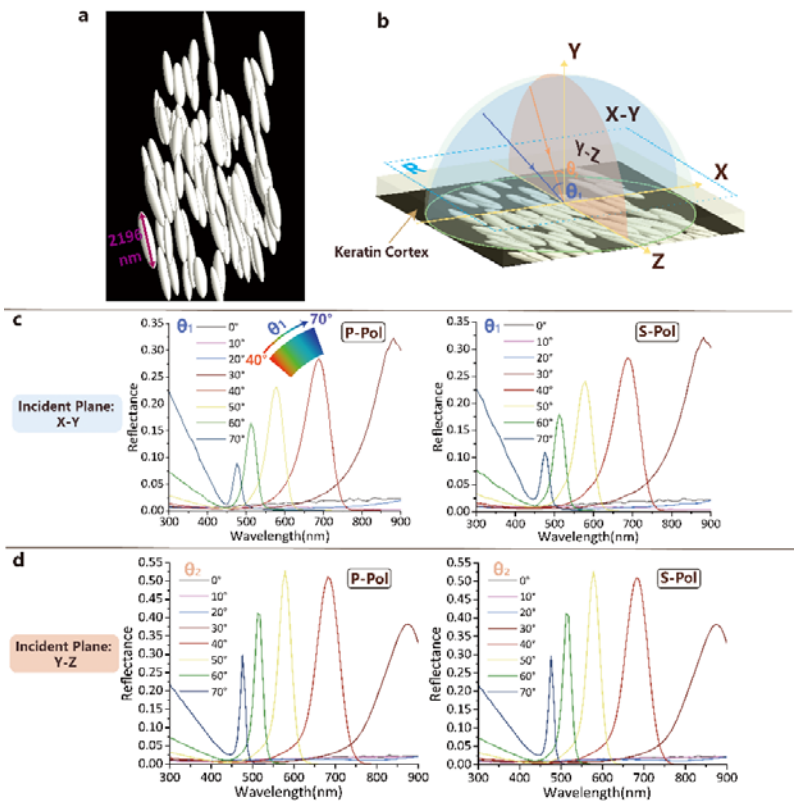

Figure 4. FDTD modeling results. (a) Representative multilayer melanosome model; (**b**) Schematic drawing of the reflectance calculation setup of the feather barb. X-Y incident plane (blue) is perpendicular, and the Y-Z incident plane (orange) is parallel to the special melanosome longitudinal axis. θ_1 and θ_2 are incident angles in X-Y and Y-Z incident planes, respectively. The blue dashed box (R) indicates the area where the reflection spectra are simulated and calculated. (**c**) Angle-dependent reflectance spectra calculated

for p- and s-polarized light by FDTD modeling with X-Y incident plane. (**d**) Angle-dependent reflectance spectra calculated for p- and s-polarized light by FDTD modeling with Y-Z incident plane. Keratin cortex layer was considered in the modeling.

Supplementary Materials